Temperature spectra from a turbulent thermal plume by ultrasound scattering

J.C. Elicer-Cortés [a,*], R. Contreras [a], D. Boyer [b], M. Pavageau [c], R.H. Hernández [a]

[a] *Departamento de Ingeniería Mecánica, Universidad de Chile, Beauchef 850, 5° Piso, Casilla 2777, Santiago, Chile*
[b] *Instituto de Física, Universidad Nacional Autónoma de México, Apartado Postal 20-364, 01000 México D.F., Mexico*
[c] *Ecole des Mines de Nantes, GPEA, UMR, CNRS 6144, DSSE, 4 rue Alfred Kastler, B.P. 2072246, F-44307 Nantes Cedex 3, France*

Abstract

This paper reports the results of a study on temperature inhomogeneities conducted on a thermal plume by using ultrasound scattering as a non-intrusive measurement technique. The plume rises from a metallic disk which can be heated up to 800 °C. The working fluid is air at atmospheric pressure. In the measurement technique, an incoming ultrasound wave is emitted towards the thermal plume. The incident wave is scattered because of non-linear couplings with the flow instabilities present in the measurement region. The scattered wave carries information about those flow instabilities. The technique allows for the retrieving of this information. The shape of the obtained spectrum of temperature fluctuations as a function of wave vector modulus $|\vec{q}| = q$ is consistent with previous theoretical analysis. Three qualitatively different regions were identified: first, a *production region* characterized by a q^2 law; secondly, a region with behavior as per q^{-3} associated with a *buoyancy region* and; finally, a *dissipation region* associated with a q^{-7} law. These spectral regions characterize the energy transfers mechanisms among the length scales of flow investigated here. A coefficient of anisotropy γ was defined to analyze anisotropic features of the flow.

Keywords: Thermal plume; Temperature spectra; Turbulence; Ultrasound scattering

1. Introduction

Thermal plumes are present in many practical and industrial applications: chemical releases to the atmosphere, industrial stacks, cooling towers, etc. Example of free convection can also be found in geophysics. Improvement of industrial processes or situations where thermal aspects are of utmost importance, i.e. where buoyancy is the driving mechanisms (fire safety for instance), require a deep understanding of the behavior and structure of heated flows. Therefore, for a number of decades thermal plumes have been the subject of many theoretical and experimental investigations. But still, a certain number of open questions remain.

Moreover, pure thermal plumes are excellent test flows to better understand the couplings that exist between the temperature and velocity fields in heated flows. It allows focusing on buoyancy effects since shear mechanisms are comparatively negligible in the production of turbulent energy. Information on the velocity field can be obtained from an analysis of the temperature field only if the studied flow is not too complex: in particular, this entails that compressibility effects can be neglected, i.e. that the nullity of the velocity divergence can be assumed. Although this is a common hypothesis in the analysis of thermal plumes, note that this has been disputed for slightly heated flows of large dimension (like flows in cooling towers for example) by Pavageau and Rey [1].

Thermal plumes are laminar in a limited number of cases only. This is due to the unstable nature inherent to such flows. One key question is still when and how a thermal plume turns turbulent and how transport phenomena are influenced. This is an important point that deserves attention as regards industrial aspects. The success of analytical and numerical analysis is generally limited by the complex nature of turbulent flows. Therefore, experiments are a useful tool in these studies

* Corresponding author. Tel.: +56-2-678-45-42; fax: +56-2-698-84-53.
E-mail address: jelicer@cec.uchile.cl (J.C. Elicer-Cortés).

Nomenclature

A	amplitude of scattering peak, V
A_{dB}	amplitude of scattering peak, dB
A_{FR}	amplitude of frequency response of transducers, V
$A_{\mathrm{FR_{dB}}}$	amplitude of frequency response of transducers, dB
A_{n}	normalized amplitude of scattering peak
B	function of variables θ, $\vec{r}$ and v
C	function of variables θ, $\vec{r}$ and v
c	speed of sound, m/s
D	diameter of the disk heated source, m
e	2.71828...
E_T	normalized spatial spectrum of temperature fluctuations
$\widetilde{E}_T$	spatial spectrum of temperature fluctuations, $\mathrm{K^2\,m^3}$
$\widetilde{E}_{T,\mathrm{axial}}$	spatial spectrum of temperature fluctuations (reception axial of receiver), $\mathrm{K^2\,m^3}$
$\widetilde{E}_{T,\mathrm{radial}}$	spatial spectrum of temperature fluctuations (reception radial of receiver), $\mathrm{K^2\,m^3}$
F	function of variables θ, $\vec{r}$ and v
$\vec{g}$	uniform gravitational field, $\mathrm{m/s^2}$
g	9.81, $\mathrm{m/s^2}$
i	$\sqrt{-1}$
I	ultrasound scattering intensity, $\mathrm{Pa^2}$
$\vec{k}$	wave vector, 1/m
$\vec{k}_{\mathrm{s}}$	scattering direction wave vector, 1/m
$\vec{k}_{\mathrm{i}}$	incoming direction wave vector, 1/m
l	characteristic length scale of flow, m
l_T	characteristic length scale of flow due to temperature fluctuations, m
l_U	characteristic length scale of flow due to vorticity, m
P_0	pressure amplitude of the incoming sound wave, Pa
p_{inc}	pressure of the incoming sound wave, Pa
$\tilde{p}_{\mathrm{scat}}$	total scattering pressure Fourier transform in space and time, $\mathrm{Pa\,m^3\,s}$
$\tilde{p}_{\mathrm{scat}}^{\mathrm{temp}}$	scattering pressure Fourier transform in space and time due to temperature fluctuations, $\mathrm{Pa\,m^3\,s}$
$\tilde{p}_{\mathrm{scat}}^{\mathrm{vort}}$	scattering pressure Fourier transform in space and time due to vorticity, $\mathrm{Pa\,m^3\,s}$
Pr	Prandtl number ($=\eta/\alpha$)
$\vec{q}$	wave vector, 1/m
q	magnitude of wave vector, 1/m
$\vec{q}_r$	wave vector in the transverse cylindrical coordinate, 1/m
$\vec{q}_z$	wave vector in the axial cylindrical coordinate, 1/m
r	transverse cylindrical coordinate, m
Ra_D	Global Rayleigh number based on diameter and temperature of disk ($=g\beta(T_{\mathrm{d}}-T_\infty)D^3/\alpha\eta$)
Ra_z	Local Rayleigh number based on height and centerline temperature excess ($=g\beta(T_{\not\subset}-T_\infty)z^3/\alpha\eta$)
s	specific entropy, J/kg K
$\widetilde{S}$	Fourier transform in space and time for two-point correlation of entropy, $\mathrm{J\,K^{-2}\,m^3\,s}$
$\widetilde{S}_k$	Fourier transform in space and time for two-point correlation of entropy–vorticity, $\mathrm{J\,K^{-1}\,m^3}$
$\widetilde{S}_k^*$	conjugated complex Fourier transform in space and time for two-point correlation of entropy–vorticity, $\mathrm{J\,K^{-1}\,m^3}$
$\widetilde{S}_{kl}$	Fourier transform in space and time for two-point correlation of vorticity, $\mathrm{m^3\,s}$
t	time, s
$\widetilde{T}$	Fourier transform in space and time of temperature fluctuations, $\mathrm{K\,m^3\,s}$
T_{d}	temperature of the heated disk, K
T_0	mean temperature of flow, K
$T_{\not\subset}$	local centerline plume temperature ($=T(r=0,z)$), K
T_∞	quiescent medium fluid temperature, K
T'	temperature fluctuations, K
$\overline{T'^2}$	mean square of temperature fluctuations, $\mathrm{K^2}$
$\vec{u}$	velocity field of flow associated with vorticity, m/s
$\vec{U}$	mean advection velocity in measurement zone, m/s
U	modulus of the mean advection velocity ($=\lvert\vec{U}\rvert$), m/s
u'	velocity fluctuations, m/s
$\vec{V}$	velocity field of flow in the coupling process with sound, m/s
$\vec{V}_{\mathrm{inc}}$	velocity field of incident sound wave, m/s
$\vec{V}_0$	velocity field amplitude of incident sound wave, m/s
$\vec{V}_{\mathrm{s}}$	velocity field associated with sound, m/s
$\vec{x}$	position vector of receiver transducer with respect to measurement volume, m
z	axial cylindrical coordinate, m

Greek symbols

α	molecular thermal diffusivity, $\mathrm{m^2/s}$
β	volumetric coefficient of thermal expansion, 1/K
γ	coefficient of the isotropy degree
δ	differential operator of a variable
Δv	scattering Doppler shifting [$=(v-v_0)$], 1/s
θ	scattering angle, rad

η	kinematic viscosity, m^2/s	ρ_0	mean density of flow without interaction, kg/m^3
v	scattered sound wave frequency, 1/s	ρ'	density fluctuations associated to sound interaction, kg/m^3
v_0	incoming sound wave frequency, 1/s	$\vec{\omega}$	vorticity distribution, 1/s
λ	wavelength scale of acoustic field, m	$\tilde{\vec{\omega}}$	Fourier transform in space and time of vorticity, m^3
π	3.14159...		
ρ	density of flow interacting with sound, kg/m^3		

in order to overcome the actual limitations of analytical and numerical approaches.

Studying thermal plumes entails the understanding of the phenomenon itself, flow regimes, buoyancy influence, and turbulent transport and production phenomena. The understanding of these phenomena can be based on spectral analysis according to the energy cascade concept developed by Kolmogorov and Obukhov in the 1940's.

In the present case, practical difficulties associated with the use of classical intrusive measurement probes prevent us from determining space and time correlations prior to spectral analysis. Recall that space and time correlations are related to each other through the Taylor hypothesis. However, this requires the assumption that turbulence is homogeneous and isotropic. Moreover, it has been shown that the Taylor's hypothesis does not necessarily apply to temperature scales or, at least, that the convection velocity of temperature structures may substantially differ from the convection velocity of dynamic structures. A factor of 3 between both convection velocities could be measured in heated grid turbulence [2]. Finally, recall that the Taylor's hypothesis theoretically applies for the turbulence scales close to the Taylor microscale and that it a priori fails for the larger and finer structures. The traditional measurement techniques (probes, fine thermocouples, LDA) corresponding to point measurements involve also restrictions due to extended experimentation periods and flow disturbances. Therefore, non-intrusive and global measurement techniques (simultaneous analysis in a finite control volume of flow) may be preferred in some cases, especially if the Taylor's hypothesis does not need to be invoked. This was so in the present work.

Over the past six decades, Obukhov [3], Lighthill [4], Kraichnan [5], Chu and Kovásznay [6], Tatarskii [7] and Baerg and Schwarz [8], among others, have conducted important research contributing to the development of a new, non-intrusive, and global in real space measurement technique based on ultrasound scattering from turbulent flows. In the analysis reported by Chu and Kovásznay [6], six different kinds of interactions can be obtained by combining three modes: acoustic, vorticity and entropy. The scattering process results from the acoustic mode coupling non-linearly with vorticity, $(\vec{u}\cdot\nabla)\vec{V}_s + (\vec{V}_s\cdot\nabla)\vec{u}$, or entropy $(\vec{V}_s\cdot\nabla)s$ modes. The flow velocity field is denoted by: $\vec{V} = \vec{V}_s + \vec{u}$, where $\vec{u}$ is associated with the essentially incompressible background flow $(\nabla\cdot\vec{u} = 0)$ and $\vec{V}_s$ is associated with the sound wave propagating through it $(\nabla\wedge\vec{V}_s = 0)$. The vorticity field in the absence of sound is: $\vec{\omega}(\vec{x},t) = \nabla\wedge\vec{u}$. Sound and flow couple when the acoustic wavelength (λ) and the characteristic length scale of the flow (l) have the same order of magnitude $(\lambda\sim l)$; i.e. when acoustic scattering occurs.

The ultrasound scattering technique has proven to be a useful tool to study turbulent flows. Indeed, experimental studies have been conducted to validate theoretical predictions. Baudet et al. [9], using a Von Kármán vortex street as a test flow (isothermal case) obtained a two-peak spectral signal: one central peak related with the incoming ultrasound wave frequency (v_0), and a shifted peak (scattering peak resulting from the wave-vorticity coupling). This frequency shift (Doppler effect) agreed with the vortex shedding Strouhal frequency. Pinton et al. [10] in a two-dimensional thermal plume (non-isothermal case) obtained a spectrum with a peak for the incoming wave and a second shifted peak revealing interaction with temperature fluctuations. Petrossian and Pinton [11] used this technique with a weakly heated turbulent air jet, in a backscattering disposition $(\theta > 90°)$ of ultrasound transducers, in order to attenuate the reception of scattering from vorticity and to take into account temperature fluctuations contribution only. They considered temperature as a passive scalar and verified the existence of an inertial-convective subrange ($-5/3$ law). Recently, Elicer-Cortés et al. [12,13] provided experimental evidence for ultrasound scattering in a turbulent thermal plume: they verified some theoretical predictions of Lund and Rojas [14] and Contreras and Lund [15]. In addition, the turbulence transition and the fully developed turbulence zones have been identified and defined rather accurately. Results were in good agreement with those obtained by traditional techniques.

The present paper reports results of a study of the fine structure of a thermal plume using ultrasound scattering. A scattering signal analysis was developed to obtain the energy spectra of temperature fluctuations and to identify the spectral regions characterizing the energy

transfer between average flow structures at different scales. Moreover, an isotropy analysis over a certain range of temperature scales is reported. This work shows evidence that our acoustic technique is useful to detect and characterize temperature structures in turbulent buoyancy driven flows.

2. Recalls on ultrasound scattering

An ultrasound scattering experiment from a turbulent thermal plume can be seen as a non-isothermal vorticity distribution $\vec{\omega}(\vec{x},t)$ [15] hit by an incoming ultrasound plane wave with velocity $\vec{V}_{\text{inc}}(\vec{x},t)=\vec{V}_0\cos(\vec{k}\cdot\vec{x}-2\pi\nu_0 t)$ and pressure $p_{\text{inc}}(\vec{x},t)=P_0\cos(\vec{k}\cdot\vec{x}-2\pi\nu_0 t)$. The amplitudes of the velocity and of the pressure associated with the incident wave are chosen such that they are small compared to the flow characteristic velocity and pressure respectively. In addition, the frequency of the incoming wave (ν_0) is tuned to be much higher than any characteristic frequency of the flow, so that the flow can be considered as stationary compared to the wave. High frequency and small amplitude waves can thus be seen as small perturbations that neither destroy nor disturb the structure of the flow.

Based on the analysis of Chu and Kovásznay [6], Lund and Rojas [14] and Contreras and Lund [15] obtained analytical expressions for the scattered acoustic pressure from vorticity and entropy modes. The scattered signal can be detected by an acoustic transducer located in an appropriate direction θ (see Fig. 1). The signal contains the contribution of two effects each with different angular dependence: sound-vorticity coupling and sound-temperature fluctuations coupling ($\tilde{p}_{\text{scat}}=\tilde{p}^{\text{vort}}_{\text{scat}}+\tilde{p}^{\text{temp}}_{\text{scat}}$). These contributions are as follows:

$$\tilde{p}^{\text{vort}}_{\text{scat}}(\vec{x},\nu)=\frac{\mathrm{i}\rho_0\pi^2\nu e^{\mathrm{i}\frac{\nu|\vec{x}|}{c}}}{c|\vec{x}|}\left(\frac{-\cos\theta}{1-\cos\theta}\right)(\vec{V}_0\wedge\hat{x})\cdot\tilde{\vec{\omega}}(\vec{q},\nu-\nu_0) \tag{1}$$

$$\tilde{p}^{\text{temp}}_{\text{scat}}(\vec{x},\nu)=\frac{\rho_0|\vec{V}_0|\pi^2\nu^2 e^{\mathrm{i}\frac{\nu|\vec{x}|}{c}}}{cT_0|\vec{x}|}\cos\theta\,\widetilde{T}(\vec{q},\nu-\nu_0) \tag{2}$$

Fig. 2 shows qualitatively the angular dependence of $\tilde{p}^{\text{vort}}_{\text{scat}}$ and $\tilde{p}^{\text{temp}}_{\text{scat}}$, assuming that both pressures are of same order of magnitude. At large angles, temperature fluctuations dominate the signal and can therefore been studied separately from the vorticity field [9–15].

Contreras and Lund [15] support that Eqs. (1) and (2) can be used for a direct non-intrusive way of measuring vorticity and temperature fluctuations [3–11]. The technique involves point measurements in Fourier space (i.e. in $\vec{k}$ space) though global in real space (i.e. in $\vec{x}$ space). The scattered pressure is linearly related with the Fourier transform in space and time of vorticity $\tilde{\vec{\omega}}(\vec{q},\nu-\nu_0)$ and temperature fluctuations $\widetilde{T}(\vec{q},\nu-\nu_0)$ fields respectively, where $\vec{q}=\vec{k}_{\text{s}}-\vec{k}_{\text{i}}=(2\pi/c)(\nu\hat{x}-\nu_0\hat{s})$ is the wave vector, shown in Fig. 1. The scattering signal is composed of frequency modes close to the incoming frequency ν_0 (i.e. $\nu\approx\nu_0$; see Fig. 3). Hence, $[(\nu-\nu_0)/\nu_0)]\ll 1$ and the absolute value of the wave vector $\vec{q}$ reads: $|\vec{q}|\approx(4\pi\nu_0/c)\sin(\theta/2)$.

The usual assumptions made to derive Eqs. (1) and (2) [14,15] are: low flow Mach number (i.e. $|\vec{V}_0|\ll|\vec{u}|\ll c=2\pi\nu_0/|\vec{k}|$, where c is the speed of

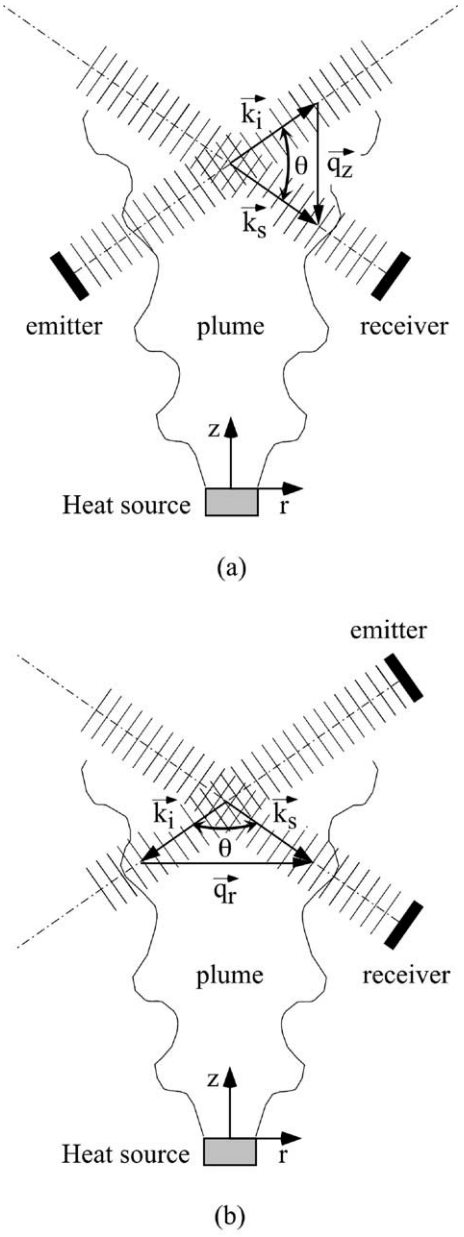

Fig. 1. Schematic representation of the non-intrusive thermal plume—ultrasound wave coupling: (a) axial configuration ($\vec{q}_z$); (b) radial configuration ($\vec{q}_r$).

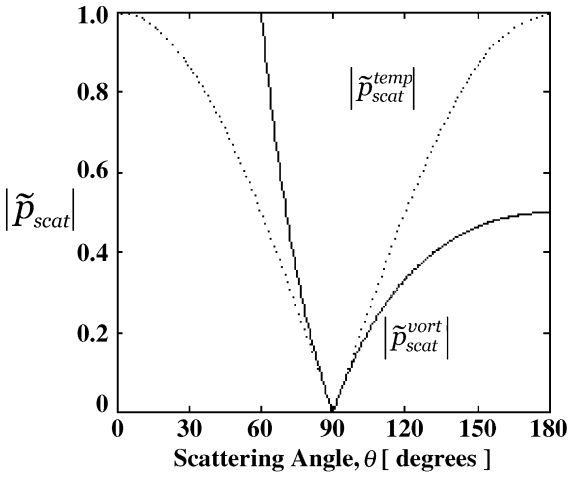

Fig. 2. The scattering angle influence on the reception of the scattering pressure by the receiver.

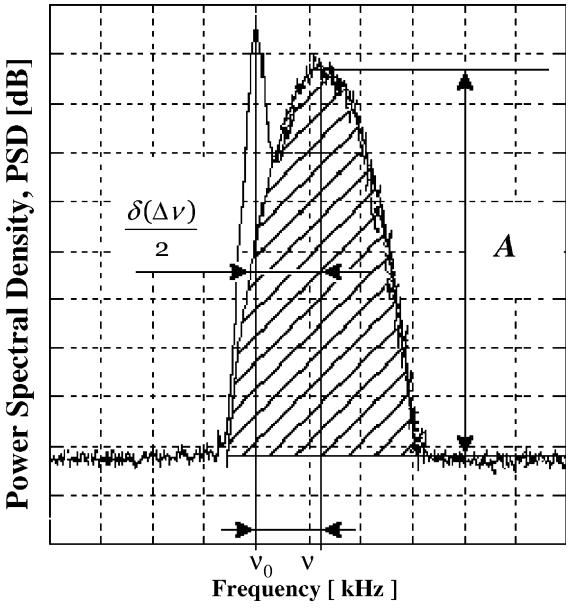

Fig. 3. Typical plot of the scattering PSD as a function of the incoming frequency.

sound); density of flow is known ($\rho = \rho_0 + \rho'$, and $\rho_0 \gg \rho'$); constant thermal conductivity; existence of a uniform gravitational field $\vec{g}$; no need for the Boussinesq approximation; sound time scale much shorter than flow time scales; flow length scales comparable to the incoming sound wave length (although turbulent flows have a wide range of length scales).

A typical acoustic spectrum of a thermal plume scattering experiment is shown in Fig. 3. The y-axis displays the power spectral density (PSD) in decibels, proportional to $|\tilde{p}_{\mathrm{scat}}(\vec{x}, \nu)|^2$, while the x-axis represents the frequency in kHz. This figure shows a peak caused by the incoming wave of frequency ν_0 and a shifted peak. The amplitude A provides information on the structure of the flow: both vorticity and thermal fluctuations through Eqs. (1) and (2) respectively. They can be reduced to temperature fluctuations only if the scattering angle θ is greater than 90°. The width $\delta(\nu - \nu_0)$ measures the related turbulence intensity; while the position of the second peak (Doppler shifting) at the frequency ν is related to the mean advection velocity of flow: $U = c(\nu - \nu_0)/2\pi \sin(\theta/2)$. In our experimental conditions, advection velocities U ranging from 0.65 to 0.75 m/s were estimated.

Keeping the angle of scattering θ constant as well as the measurement height (z/D), the wave vector $\vec{q}$ solely depends on the incoming frequency ν_0 and scans flow inhomogeneities of characteristic length scale l given by: $|\vec{q}| \approx (4\pi\nu_0/c)\sin(\theta/2) \approx (2\pi/l)$. It is therefore possible to choose the scale l at which we wish to observe the flow by tuning the frequency ν_0. A priori, scattering is produced by velocities (vortices) and temperature inhomogeneities of length scales l_U and l_T respectively. Taking into account that $Pr \approx 0.7$, these length scales should not be very different ($l_U \approx l_T$).

A tunable wavelength represents a significant advantage in this technique, since it enables selecting a turbulence scale by just tuning the incoming sound wave frequency. Accuracy is limited by diffraction effects [10]. A good spectral resolution is obtained at the expense of real space resolution. The separation of vorticity and temperature effects mentioned above was checked in other experimental studies [9,10]. Unlike Eulerian point measurements, the acoustic ones offer a global characterization of flow inhomogeneities in a finite volume, which provides a way of decomposing the flow into space modes, i.e. it sorts out the unstable modes or vortices according to their size. For instance, this is particularly interesting in the case of flows characterized by roughly periodic structures. A lot of flow statistics within a finite volume can be obtained in a short time. It is the case in Lagrangian type measurements. Measurements at fixed $|\vec{q}|$ consist in recording a signal over an extended period time. The PSD plot for a given $|\vec{q}|$ as shown in Fig. 3, results from data acquisition over time. We can schematically decompose turbulent flows into time averaged structures representing inhomogeneities of well defined size, $l \approx 2\pi/|\vec{q}| \approx [c/2\nu_0 \sin(\theta/2)]$. If no structures of a given size were present, the associated PSD plots would be flat.

As detailed by Elicer-Cortés et al. [13], acoustic transducers are band-pass filters with frequency responses varying with the incoming wave frequency ν_0, the distance between the transducers and the scattering angle θ. It is necessary to get rid of these variations in order to compare the scattering peaks at different frequencies. This is achieved by normalizing the frequency of transducers for each configuration. For a given configuration, the scattering peak $A(\nu_0)$ and the related frequency response $A_{\mathrm{FR}}(\nu_0)$ amplitude vary with ν_0 only.

Their expression in decibels is as follows: $A_{\mathrm{dB}} = 10\log_{10} A^2$ and $A_{\mathrm{FR_{dB}}} = 10\log_{10} A_{\mathrm{FR}}^2$. The normalization consists in making the quotient of the two amplitudes in such a way the normalized amplitude, A_{n}, will only depend on flow properties $(T_{\mathrm{d}}, z/D)$:

$$A_{\mathrm{n}} = \frac{A}{A_{\mathrm{FR}}} = \frac{10^{\frac{A_{\mathrm{dB}}}{20}}}{10^{\frac{A_{\mathrm{FR_{dB}}}}{20}}} \tag{3}$$

3. Methodology for obtaining energy spectra

Lund and Rojas [14] and Contreras and Lund [15] found an analytical expression for the ultrasound scattered intensity $I(\vec{x}, v)$ as a function of the Fourier transform in space and time of the two-point correlations of: vorticity $\widetilde{S}_{kl}(\vec{q}, v - v_0)$; entropy $\widetilde{S}(\vec{q}, v - v_0)$; entropy–vorticity $\widetilde{S}_k(\vec{q}, v - v_0)$ and; its conjugated complex $\widetilde{S}_k^*(\vec{q}, v - v_0)$. Lund and Rojas [14] relate $I(\vec{x}, v)$ with $|\tilde{p}_{\mathrm{scat}}(\vec{x}, v)|^2$ so that it is possible to write:

$$\begin{aligned} |\tilde{p}_{\mathrm{scat}}(\vec{x}, v)|^2 \propto I(\vec{x}, v) &= B(\theta, \vec{x}, v)\widetilde{S}_{kl}(\vec{q}, v - v_0) \\ &+ C(\theta, \vec{x}, v)\widetilde{S}(\vec{q}, v - v_0) + \cdots + F(\theta, \vec{x}, v) \\ &\times \left[\widetilde{S}_k(\vec{q}, v - v_0) - \widetilde{S}_k^*(\vec{q}, v - v_0)\right] \end{aligned} \tag{4}$$

In Fig. 1 we note that the wave vector can be either axial $(\vec{q}_z)$ or radial $(\vec{q}_r)$ depending on the configuration of the transducers. Fig. 4 shows the normalized values of the two-point correlations with respect to the maximum value of $\widetilde{S}(\vec{q}, v - v_0)$. The scattered intensity for angles $\theta > 90°$ is dominated by the two-point correlation function of entropy fluctuations, $|\tilde{p}_{\mathrm{scat}}(\vec{x}, v)|^2 \propto I(\vec{x}, v) \approx C(\theta, \vec{x}, v)\widetilde{S}(\vec{q}, v - v_0)$, so that the signal observed in this range is equivalent to the Fourier transform in space

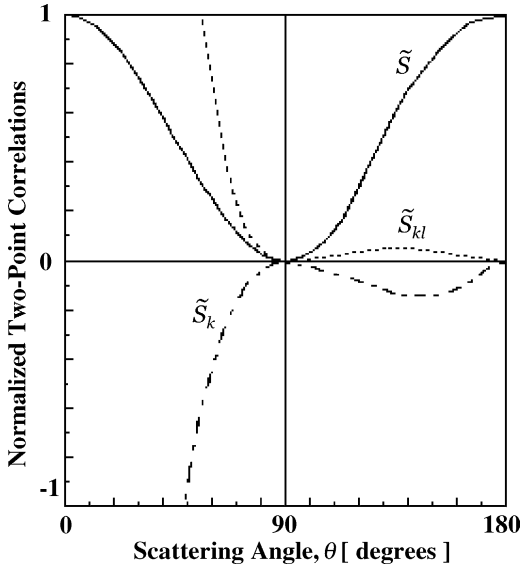

Fig. 4. Relative importance of the normalized two-point correlations terms of the intensity of ultrasound scattering.

and time of two-point temperature fluctuations $\widetilde{S}(\vec{q}, v - v_0) = \overline{\widetilde{T}(\vec{q}, v)\widetilde{T}(-\vec{q}, -v)}$. Thus, the mean square value of temperature fluctuations $\overline{T'^2}$ is obtained by the inverse Fourier transform in space and time of the spectrum:

$$\overline{T'^2} = \int\int \frac{\overline{\widetilde{T}(\vec{q}, v)\widetilde{T}(-\vec{q}, v)}\,\mathrm{d}q\,\mathrm{d}v}{2\pi} = \int \widetilde{E}_T(\vec{q})\,\mathrm{d}q \tag{5}$$

Therefore:

$$\widetilde{E}_T(\vec{q}) = \int \frac{\widetilde{S}(\vec{q}, v)}{2\pi}\,\mathrm{d}v \tag{6}$$

For the axial and radial configurations of Fig. 1, spectra can be written respectively as:

$$\widetilde{E}_{T,\mathrm{axial}}(\vec{q}_r = 0, \vec{q}_z) = \int \frac{\widetilde{S}(\vec{q}_r = 0, \vec{q}_z, v)\,\mathrm{d}v}{2\pi} \tag{7}$$

$$\widetilde{E}_{T,\mathrm{radial}}(\vec{q}_r, \vec{q}_z = 0) = \int \frac{\widetilde{S}(\vec{q}_r, \vec{q}_z = 0, v)\,\mathrm{d}v}{2\pi} \tag{8}$$

Using Eq. (6), we can obtain the temperature spectrum from the scattering peak by integration over the hatched area in Fig. 3, for each wave vector $\vec{q}$. The estimated mean error attributed to the choice of integration limits in Fig. 3 was about 3%. The error was estimated by dividing the standard deviation by the average value of integration of the hatched area of that figure, and that was done for twenty realizations of the numerical integration procedure.

As each temperature fluctuations spectrum is normalized by the frequency response of the transducers, we plot the results in terms of these relative values $E_T(\vec{q}) = E_T(v_0) \propto \widetilde{E}_T(\vec{q})$; the contents of the physics of scattering should remain unaltered. The goal of this experiment is to characterize energy transfers through the average structures of the flow from the analysis of $E_T(\vec{q})$. In a given measurement volume, if temperature fluctuations were isotropic, one would have $\overline{T'^2} = \overline{T'^2}_{\vec{q}_z=0} = \overline{T'^2}_{\vec{q}_r=0}$, or $E_T = E_{T,\mathrm{axial}} = E_{T,\mathrm{radial}}$. It is then possible to define the correlation γ:

$$\gamma = \frac{E_{T,\mathrm{axial}} \cdot E_{T,\mathrm{radial}}}{(E_{T,\mathrm{axial}})^2 + (E_{T,\mathrm{radial}})^2} \tag{9}$$

which can be interpreted as a measure of the degree of isotropy of the system. It is such that $\gamma = 0.5$ for the isotropic case.

4. Experimental setup and measurement technique

Details regarding the experimental setup have been given by Elicer-Cortés et al. [12,13,16]. However, some essential aspects of it are recalled here. The apparatus consisted of a thermal source immersed into quiescent air at atmospheric pressure inside a 1.8×1.8 m^2 square

base and 2.5 m high anechoic enclosure with wooden walls. The anechoic properties of the enclosure were achieved after covering the internal walls with flexible polyurethane sheets with the following characteristics: capacity of absorption over 90% for frequencies above 1 kHz, material density of 30 kg/m^3, elasticity of up to 135% and thermal conductivity of 0.25 W/(m K). External noises and echoes could thus be reduced satisfactorily [12]. The investigated axisymmetric thermal plume was generated by an 8 mm thick round metallic disk of diameter $D = 80$ mm. The disk could be heated electrically up to 800 °C by a regulated AC power supply of 1 kV A. The heat release rate from the hot active surface of the disk ranged from 0 to 400 W. It allowed us to achieve turbulent flow regimes if desired. A thermocouple (K type) located only 0.3 mm below the active surface allowed accurate measurements of the temperature at the disk surface. The lower part of the source was thermally insulated with 2.54 cm thick layers of rigid fiber (Thermotec LD-2300). A still air chamber was built at the top of the anechoic enclosure for the warm air to eventually leave the enclosure and not to recirculate within it. Holes were provided through the lower part of the enclosure walls to allow admission of fresh air. All holes were covered with synthetic fiber wool to avoid air blasts from the exterior. The enclosure was located in the basement of our experimental laboratory to avoid global warming of the ambient air during daytime and to reduce possible influence of external noises. Thus, the present arrangement allowed the generation of almost ideal thermal plumes developing in an "infinite" adiabatic ambient fluid at rest. As previously stated [13,16], air within the enclosure was not stratified. This was checked by means of five thermocouples distributed uniformly with respect to height, every 0.5 m.

Both the transmitter and the receiver are acoustic transducers of the Sell type [17] of 15 cm diameter, similar to those used in earlier investigations [10–13]. Acoustic transducers are assembled on supports allowing vertical, horizontal and angular displacements (to select the scattering angle θ). Transducers respond from 5 to 100 kHz and the typical amplitude of the incoming sound wave remains weak; it is about $P_0 \approx 1$ Pa. This corresponds to $|\vec{V}_{\text{inc}}| \approx 0.2$ cm/s, much smaller than the typical flow velocity. A twin DC power supply of high tension (0–400 V) provides a polarization tension of 270 V to each transducer.

Fig. 5 helps to understand the experimental arrangement and how data of scattering experiments were captured. A sinusoidal signal of high frequency is generated by an HP-33120A function generator, which is amplified in a NF-4005 power amplifier and sent to the transmitter transducer. This transmitter delivers a plane ultrasound wave, which couples with the flow and scatters sound. The receiver transducer detects the complex and time-varying scattered signal (amplitude and phase) [12]. This signal corresponds to the Fourier transform in space of vorticity and/or temperature fluctuations. The receiver converts the acoustic pressure into electric charges proportional to pressure and sent them to a BK-2635 charge amplifier, which returns a voltage signal. This signal is received by a two-channel Lock-in amplifier SR-830. Narrow band frequency modulation eliminates from the signal the components that have frequencies very different from the reference frequency (i.e. $v_0 \pm \Delta v$), where Δv corresponds to the Doppler shift. The Lock-in amplifier delivers a complex signal sampled and recorded on a Pentium PC provided with an AT-A2150C acquisition board (16 bits AN converter and antialiasing filter) and an AT-GPIB controller card. Signal processing was achieved after development of appropriate Matlab programs. One finally gets the contributions of vorticity and/or temperature fluctuations of the scattering process in terms of PSD distributions, i.e. the Fourier transform in space and time of the signal (see Fig. 3). More details can be found in recent papers [12,13].

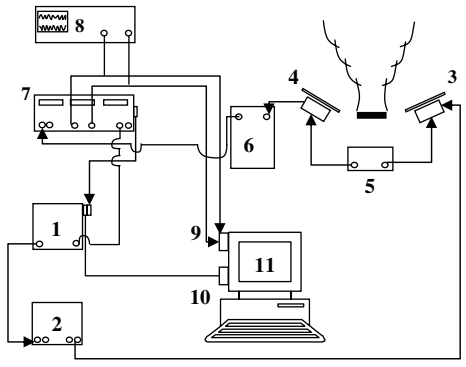

Fig. 5. Disposition of the instruments: (1) function generator; (2) power amplifier; (3) acoustic transmitter; (4) acoustic receiver; (5) twin DC power supply; (6) charge amplifier; (7) Lock-in amplifier; (8) analog oscilloscope; (9) acquisition board card; (10) GPIB controller card; (11) Pentium PC.

5. Results and discussion

Obtaining the energy spectrum of temperature fluctuations requires a wide range of incoming wave frequencies v_0 (or wave vector $\vec{q}$), in order to access information on a wide range of turbulent scales. However, the incoming frequency must be compatible with the frequency response of transducers (v_0, from 5 to 100 kHz). Experiments were conducted under the following conditions: we chose $\theta = 130°$ in order to enhance the contribution coming from temperature fluctuations at the expense of vorticity contribution; measurements with both axial and radial arrangements of the transducers were performed. In order to use the best frequency response of transducers [13] we worked

with frequencies v_0 ranging from 20 to 80 kHz. This corresponded to a wave vector modulus q ranging from 670 to 2680 m^{-1}, i.e. temperature length scales l_T ranging from 9.4 to 2.3 mm, respectively. Measurement heights downstream of the thermal source were chosen so that we could observe transition and developing turbulence regimes [13]. This corresponded namely to heights of 60 cm ($z/D = 7.5$) and 80 cm ($z/D = 10$). Finally, for both heights, disk temperatures were $T_d = 500$ and 700 °C. For these two temperatures used in our experiments, the global Rayleigh numbers based on the disk diameter D were $Ra_D = 1.09 \times 10^6$ and $Ra_D = 6.83 \times 10^5$ respectively. In order to take into account the local characteristics of the investigated flow and to be able to compare with experiments carried out with other working fluids, the results are presented using local Rayleigh numbers based on the height z. This height is determined from the position of the center of the measurement volume. For the temperatures and heights considered in our experiment, local Rayleigh numbers range from $Ra_z = 1.87 \times 10^8$ to $Ra_z = 3.84 \times 10^8$.

Fig. 6 shows the plot of the normalized amplitude (A_n) of the scattering peak as a function of the incoming wave frequency v_0. Measurements errors are indicated in relative terms in this figure. This configuration ($T_d = 500$ °C and $z/D = 7.5$) has been chosen as a typical situation for which the flow is unstable. As the frequency v_0 increases, i.e. for smaller structures, the normalized amplitude tends to decrease. This behavior is consistent with the usual cascade scenario toward small length scales. Elicer-Cortés et al. [13] have reported similar curves, obtained for different disk temperatures and measurement heights. It is generally observed that energy production resulting from temperature fluctuations increases as the heating temperature increases. The slope of the curve (in Log–Log coordinates) in the high frequency domain may vary when the scattering angle varies, since the relative strength of vorticity and temperature spectra is sensitive to the scattering angle. When the angle is $\theta = 130°$, the scattering peak is essentially and linearly related to the Fourier transform in space and time of temperature fluctuations $\widetilde{T}(\vec{q}, v - v_0)$; in such a case the observed slope is close to −3/2. As the wave vector modulus is proportional to the incoming frequency ($|\vec{q}| \propto v_0$), the scattered pressure may be expressed as $\tilde{p}_{scat} \propto q^{-3/2}$ and thus, $\widetilde{T} \propto q^{-3/2}$. Pinton et al. [10] obtained similar results in experiments conducted on a thermal plume originating from a two-dimensional heat source.

A typical spectrum of temperature fluctuations revealing the behavior of the flow is illustrated in Fig. 7, corresponding to an experimental configuration where the disk temperature is $T_d = 700$ °C and the height measurement $z/D = 10$. The scatter of data results from measurement errors.

Three spectral regions can be identified in Fig. 7. The first region is a *production region*, where temperature spectra are characterized by a law q^2. Production is here due to turbulent flux ($2g\beta\overline{u'T'}$). The second region is quite interesting and is characterized by a law q^{-3}, corresponding to a *buoyancy region*, typical in buoyant free convection flows. Such behavior has already been reported by Lumley [18] in a spectral analysis of quasi-inertial turbulent flows in stably stratified environments and by several other authors for round plumes [19–22]. Such −3 power laws were observed for both passive (concentration mixture) and active scalars (temperature) in fluids characterized by Prandtl numbers ranging between 0.7 and 7. However, since the mean velocity and the temperature fields are strongly coupled in turbulent

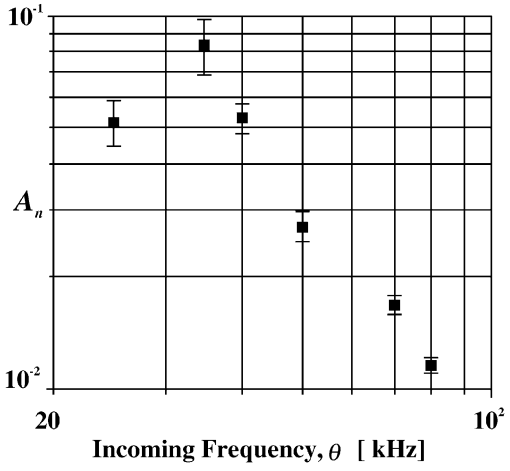

Fig. 6. Normalized amplitude of the scattering PSD versus the incoming wave frequency ($T_d = 500$ °C; $z/D = 7.5$; $Ra_z = 1.87 \times 10^8$).

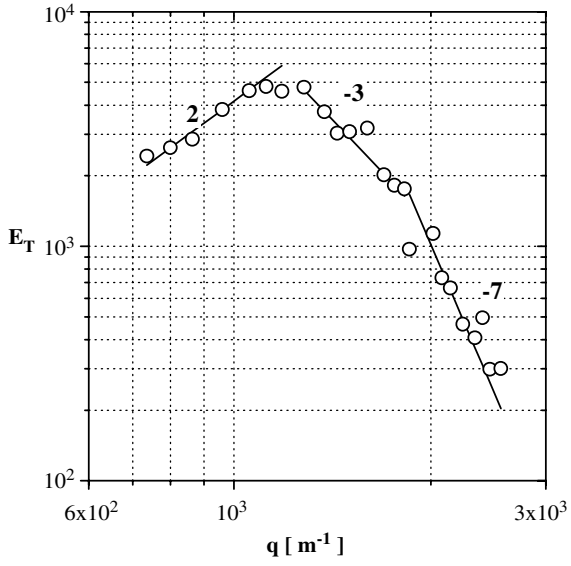

Fig. 7. Temperature spectrum as a function of wave vector ($T_d = 700$ °C; $z/D = 10$; $Ra_z = 3.84 \times 10^8$).

free convection and because relevant fluctuations are correlated, fluctuations of velocity and temperature exhibit a great degree of similarity. This implies that velocity and temperature spectra should be very similar to each other.

Rather than giving an analytical explanation of this −3 slope, we should emphasize the absence of the classical −5/3 slope (although previous studies reported such behavior). Remember that the existence of a constant −5/3 slope region is related to a hypothesis of homogeneity and isotropy. The appearance of a −3 power law region (inertial-diffusive subrange [20]) may be related with the passage in the measurement volume of large structures [19] generated by the hot source. These structures are responsible for energy transfer modes that are not present in classical turbulent shear flows. Buoyancy effects seem to impose the rate at which potential energy is converted into kinetic energy of the larger scales. Taking over viscous effects (in comparison to flows for which energy transfers are driven essentially by turbulent shear), this additionally entails noticeable modifications of the inertial equilibrium range within which energy of the larger scales is transferred to smaller scales according to the cascade concept of Kolmogorov. Our observations come very close akin to those of Kotsovinos [19] who, along the axis of a round water plume, observed a −3 spectral region in the low-frequency region (from 0.2 to 10 Hz) next to the −5/3 inertial-convection subrange. He argued that the −3 slope reflected the preferential feeding of the largest eddies by buoyancy forces. Transformation of potential energy into kinetic energy becomes more efficient with increasing the eddy size (or decreasing the wave number). Kotsovinos argued that, as larger eddies store most of the kinetic energy, the usual mechanism of transfer of energy from large to small scales does not affect the −3 slope. He admitted that both theoretical and dimensional analysis are needed to understand the modification of the power spectrum due to buoyancy forces in freely convection flows. The underlying instability problem is very complex. Although modeling turbulence with classical statistical models appears unable to describe the transverse and longitudinal evolutions of turbulent magnitudes simultaneously in thermal plumes, interesting results are reported by Zhou et al. [25] in a LES simulation of a turbulent forced plume. The velocity energy spectrum for velocity shows a −5/3 power law decay, while the power spectrum of temperature fluctuations exhibits both −5/3 and −3 power laws; the behavior of spectra is strongly driven by buoyancy forces.

In the literature, there is no complete agreement on the shape of spectra. The experiments of Dai et al. [20–22] are consistent with a −5/3 power inertial-convection decay, followed by a −3 power inertial-diffusive decay. On the other hand, Kotsovinos [19] observed spectra with a −3 power law followed by a −5/3 inertial-convective region. Moreover, the spectra with −3 slopes exhibited some discontinuities: first, a jump from a −3 to another −3 subrange, and then a jump from a −3 to a −5/3 subrange. It is actually difficult to say whether those observational differences are representative of different physical mechanisms or if they are related to the measurement techniques.

Our results are significant since they clearly illustrate the active "contaminant" role played by the temperature field in pure thermal plumes. Here, the buoyancy can be interpreted as an inhibitor of isotropy since no inertial range was identified. These findings are qualitatively different from those of Petrossian and Pinton [11], who used the same measurement technique to study a *weakly* heated turbulent air jet. These authors concluded that temperature may be considered as a passive scalar and they proved the existence of an inertial-convective subrange (−5/3 law) in the spectrum. Recall that Papailiou and Lykoudis [23] stated that spectrum shapes depend on the part of the flow produced by buoyancy instabilities, which leads to distinct spectral regions controlled by either mechanical or buoyancy energy supply. They also proposed that a *buoyancy region* would exist only if the size l_T of structures is small enough so that these structures are affected by buoyancy only but not by effects of shear stress. Pavageau [2] in free convection from a heated grid found that the inertial-convective subrange of the temperature field was narrower than expected, and that the classical −5/3 law characteristic of the inertial-convective subrange was replaced by a −2 law. This was attributed to dilatation mechanisms whose relevant effects may not be negligible in flows of large dimensions even for a weak temperature differential between the flow and the ambient fluid.

In the present study, a third region was also identified. This so-called *dissipative region*, of very fast decay, is consistent with a q^{-7} law. This kind of law was proposed from theoretical considerations by Corrsin [24] in a study on temperature fluctuation spectra for isotropic turbulent flows. In our case, this range is situated in a wave vector region with modulus $|\vec{q}| > 2000\ \mathrm{m}^{-1}$, that is, for structures sizes l_T smaller than 3 mm. The limitations with regard to the frequency response of transducers do not allow us to examine smaller scales. Present measurements were not able to resolve more decades of the space power spectra. Therefore, we cannot be so conclusive in this *dissipative region*.

Fig. 8 shows spectra corresponding to four different configurations. The spectra follow the same general behavior, thus showing the consistency of the results. The data do not depend much on the disk temperature nor the measurement height.

When buoyancy forces are the driving mechanism for motion, anisotropy is enhanced by the active scalar role of the temperature, which explains the absence of a power law −5/3. We hence focused on the larger scales,

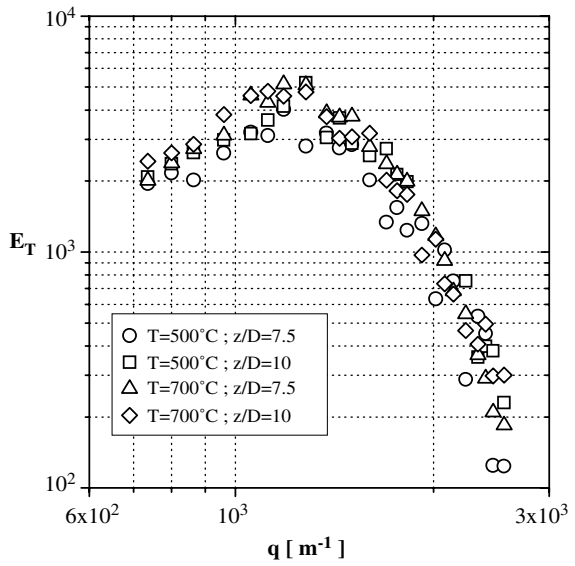

Fig. 8. Overlapping temperature spectra as a function of wave vector: –○– $Ra_z = 1.87 \times 10^8$; –□– $Ra_z = 2.86 \times 10^8$; –Δ– $Ra_z = 2.47 \times 10^8$; –◇– $Ra_z = 3.84 \times 10^8$.

which are responsible for production of turbulent energy. From estimates of the axial and radial temperature spectra, it was observed that, in general, $E_{T,\text{axial}}(\vec{q}_r = 0, \vec{q}_z)$ was greater than $E_{T,\text{radial}}(\vec{q}_r, \vec{q}_z = 0)$. This was attributed to the fact that buoyancy effects tend to develop anisotropy especially at larger scales, although one usually expects buoyancy to have less influence in the production range. By considering the ratio of $E_{T,\text{axial}}(\vec{q}_r = 0, \vec{q}_z)$ with respect to $E_{T,\text{radial}}(\vec{q}_r, \vec{q}_z = 0)$ for any given wave vector, it can be easily confirmed that relevant temperature structures exhibit a clear anisotropy. To quantify this more precisely, the γ coefficient defined earlier (Eq. (9)) has been plotted in Fig. 9: (a) with respect to wave vector $|\vec{q}|$ for some values of z/D and; (b) versus z/D for various length scales $l_T \approx 2\pi/|\vec{q}|$. It is observed that close to the hot source ($z/D = 5.0$), temperature structures are anisotropic whatever length scale considered. The isotropy degree remains almost constant and equal to 0.4. This seems to indicate that buoyancy have little influence on turbulent temperature structures whose shape and size may be controlled principally by a constant rate of strain. At higher distances from the source ($z/D = 7.5$), a very low degree of isotropy was measured for l_T equal to 20 mm, i.e. for scales preferentially sensitive to shear stress, but buoyancy effect is strong because temperature excess is still important. The coefficient γ remains almost constant and equal to 0.23 for all other temperature scales. In this case, it seems that buoyancy and shear mechanisms have simultaneously significant effects. Finally, for $z/D = 9.4$ the coefficient γ increases with decreasing temperature scale. It reaches a value close to 0.5 for the smaller scales, as expected. At this distance from the source, shear has a

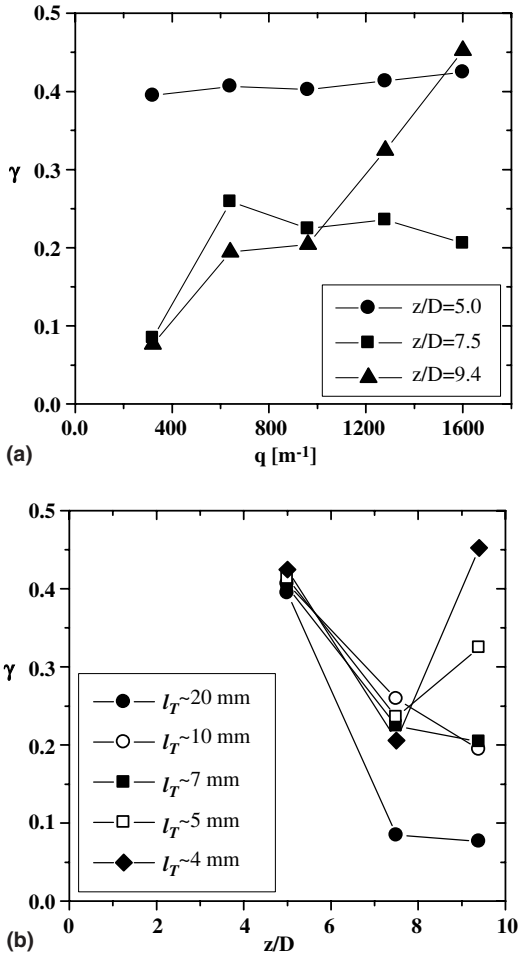

Fig. 9. Coefficient of isotropy degree as a function of: (a) wave vector $|\vec{q}|$; (b) dimensionless height (z/D).

significant effect only on the largest structures with buoyancy effects taking over on the smallest length scales (around 4 mm) as one approaches the *buoyancy region* ($l_T < 3$ mm). High values of the isotropy degree can be only explained by the reduction of buoyancy since the temperature excess becomes very weak as the distance from the hot source increases.

6. Conclusions

We have developed an experimental methodology based on the theory of ultrasound scattering by turbulent flows in order to obtain and analyze their fine structure. An important advantage of this technique is the possibility to target specific length scale via an appropriate choice of the incoming wave frequency v_0 (i.e. the wave vector $\vec{q}$). This methodology was applied to investigate the energy distribution of temperature fluctuation scales in an axisymmetric thermal plume.

Spectral distributions for temperature fluctuations were presented as functions of the wave vector modulus

(q). The spectra for temperature fluctuations obtained enabled identifying three distinct spectral regions that correspond to energy transfer mechanisms between scales: a *production region* characterized by a q^2 law and due to turbulent flux ($2g\beta\overline{u'T'}$); a *buoyancy region* characterized by a q^{-3} law, characteristic of anisotropic turbulence caused by buoyancy that modifies the inertial equilibrium range within which energy of the larger scales is transferred to smaller scales; and finally, a *dissipation region* that follows a behavior as per q^{-7}.

Higher spectra values were measured in the axial configuration with respect to radial configuration, revealing anisotropy over the whole scale range considered here. By making assumptions on the concept of isotropy and how to use the spectra on this subject, a coefficient of the isotropy degree γ was introduced ($\gamma = 0.5$ for full isotropy). This coefficient enabled the verification of the anisotropic characteristics of flow and the influence of buoyancy and shear stress.

This work may finally provide a new incentive for the use of ultrasound scattering as a non-intrusive measurement technique to detect spatial average structures in non-isothermal turbulent flows.

7. Future research needs

Further research will deal with other kinds of direct measurements in Fourier space using ultrasound scattering. In a forthcoming paper, we will investigate more in details the degree of anisotropy of a pure thermal plume, the influence of buoyancy and its role in transport mechanisms, diffusion and dissipation.

Acknowledgement

The study reported in this paper was supported by CONICYT under grant FONDECYT No 1010135 and 7010135.

References

[1] M. Pavageau, C. Rey, Observation of volume variation effects in turbulent free convection, Int. J. Heat Mass Transfer 45 (2002) 181–192.

[2] M. Pavageau, Etude expérimentale de la turbulence de grille en convection naturelle—analyse des effets non-boussinesq, Thèse de Doctorat, Université de Nantes—Ecole Centrale de Nantes, France, 1994.

[3] A.M. Obukhov, Über die Schallstreunung in der Turbulenten Strömung, Dokl. Akad. Nauk. SSSR 30 (1941) 616–620.

[4] M.J. Lighthill, On sound generated aerodynamically I, general theory, Proc. Roy. Soc. A 211 (1952) 564–587.

[5] R.H. Kraichnan, The scattering of sound in a turbulent medium, J. Acoust. Soc. Am. 25 (6) (1953) 1096–1104.

[6] B.T. Chu, L.S.G. Kovásznay, Nonlinear interactions in a viscous heat-conducting compressible gas, J. Fluid Mech. 3 (5) (1958) 494–514.

[7] V.Y. Tatarskii, Wave Propagation in a Turbulent Medium, McGraw-Hill, New York, 1961.

[8] W. Baerg, W.H. Schwarz, Measurements of the scattering of sound from turbulence, J. Acoust. Soc. Am. 39 (6) (1966) 1125–1132.

[9] C. Baudet, S. Ciliberto, J.F. Pinton, Spectral analysis of the Von Kármán flow using ultrasound scattering, Phys. Rev. Lett. 67 (1) (1991) 193–195.

[10] J.F. Pinton, C. Laroche, S. Fauve, C. Baudet, Ultrasound scattering by Buoyancy driven flows, J. Physique II France 3 (1993) 767–773.

[11] A. Petrossian, J.F. Pinton, Sound scattering on a turbulent, weakly heated jet, J. Physique II France 7 (1997) 801–812.

[12] J.C. Elicer-Cortés, C. Baudet, Ultrasound scattering from a turbulent round thermal pure plume, Exp. Therm. Fluid Sci. 18 (4) (1999) 271–281.

[13] J.C. Elicer-Cortés, J. Fuentes, A. Valencia, C. Baudet, Experimental study of transition to turbulence of a round thermal plume by ultrasound scattering, Exp. Therm. Fluid Sci. 20 (2000) 137–149.

[14] F. Lund, C. Rojas, Ultrasound as a probe of turbulence, Physica D 37 (1989) 508–514.

[15] H. Contreras, F. Lund, Ultrasound as a probe of turbulence II. Temperature inhomogeneities, Phys. Lett. A 149 (2,3) (1990) 127–130.

[16] J.C. Elicer-Cortés, Measurements of the temperature field in an axisymmetric thermal pure plume, Exp. Heat Transfer 11 (1998) 207–219.

[17] D. Anke, Luftschallwandler nach dem Sell-Prinzip für Frequenzen von 50 kHz bis 100 kHz, Acustica 30 (1974) 30–39.

[18] J.L. Lumley, The spectrum of nearly inertial turbulence in a stably stratified fluid, J. Atmos. Sci. 21 (1) (1965) 99–102.

[19] N. Kotsovinos, Turbulence spectra in free convection flow, Phys. Fluids A 3 (1) (1991) 163–167.

[20] Z. Dai, L.K. Tseng, G.M. Faeth, Structure of round, fully developed, buoyant turbulent plumes, ASME J. Heat Transfer 116 (1994) 409–417.

[21] Z. Dai, L.K. Tseng, G.M. Faeth, Velocity statistic of round, fully developed, buoyant turbulent plumes, ASME J. Heat Transfer 117 (1995) 138–145.

[22] R. Sangras, Z. Dai, G.M. Faeth, Mixing structure of plane self-preserving buoyant turbulent plumes, ASME J. Heat Transfer 120 (1998) 1033–1041.

[23] D. Papailiou, P. Lykoudis, Turbulent free convection flow, Int. J. Heat Mass Transfer 17 (1974) 161–172.

[24] S. Corrsin, On the spectrum of isotropic temperature fluctuations in an isotropic turbulence, J. Appl. Phys. 22 (1951) 469–473.

[25] X. Zhou, K.H. Luo, J.J.R. Williams, Large-eddy simulation of a turbulent forced plume, Eur. J. Mech. B—Fluids 20 (2001) 233–254.